Journal of Pathology
J Pathol 2019; **247:** 650–661
Published online 20 February 2019 in Wiley Online Library (wileyonlinelibrary.com) DOI: 10.1002/path.5223

INVITED REVIEW

New tools for pathology: a user's review of a highly multiplexed method for *in situ* analysis of protein and RNA expression in tissue

Jérémie Decalf[1], Matthew L Albert[1] and James Ziai[2]*

[1] *Department of Cancer Immunology, Genentech, Inc., South San Francisco, CA, USA*
[2] *Department of Pathology, Genentech, Inc., South San Francisco, CA, USA*

**Correspondence to: James Ziai, Department of Research Pathology, Genentech, Inc., 1 DNA Way, Mailstop 72b, South San Francisco, CA 94080, USA. E-mail: ziai.james@gene.com*

Abstract

Tumor cell heterogeneity and tumor cell–stromal interactions are being explored as determinants of disease progression and treatment resistance in solid tumor and hematological malignancies. As such, tools simultaneously capable of highly multiplexed profiling of tissues' protein and RNA content, as well as interrogation of rare or single cells, are required to precisely characterize constituent tumor cell populations, infiltrating lymphocytes and stromal elements. Access to spatial relationships will enable more precise characterization of tumors, support patient stratification and may help to identify novel drug targets. Multiple platforms are being developed to address these critical unmet needs. The NanoString digital spatial profiling (DSP) platform enables highly multiplexed, spatial assessment of protein and/or RNA targets in tissues by detecting oligonucleotide barcodes conjugated via a photocleavable linker to primary antibodies or nucleic acid probes. Although this platform enables high-dimensional spatial interrogation of tissue protein and RNA expression, a detailed understanding of its composition, function and chemistry is advisable to guide experimental design and data interpretation. The purpose of this review is to provide an independent, comprehensive description of the DSP technology, including an overview of NanoString's capture and antibody barcode conjugation chemistries, experimental workflow, data output and analysis methods. The DSP technology will be discussed in the context of other highly multiplexed immunohistochemistry methods, including imaging mass cytometry and multiplexed ion beam imaging, to inform potential users of the advantages and limitations of each. Additional issues such as preanalytical variability, sampling and specimen adequacy will be considered with respect to the platforms to inform potential experimental design.

Keywords: multiplexed immunohistochemistry; NanoString; *in situ* hybridization; tissue biomarkers; tumor microenvironment

Received 19 October 2018; Revised 6 December 2018; Accepted 14 December 2018

Conflict of interest statement: The authors are all employees of Genentech, Inc. The authors declare no conflicts of interest that may have influenced the composition of this manuscript.

Introduction

Immunohistochemistry (IHC) continues to play a central role in the clinical diagnosis and prognosis of cancer, as well as the selection of patients for targeted therapies [1–4]. These therapies, however, generally exploit cancer cell genomics or expression of unique, tumor-specific antigens, but often do not manage to integrate multiple aspects of the tumor microenvironment [5]. Nonetheless, the tumor microenvironment – its cellular composition and architecture – is increasingly recognized as a significant contributor to treatment resistance, immune evasion and tumor recurrence in the setting of both traditional chemotherapy as well as newer immunotherapies [6–9]. The promise of personalized medicine rests to a large degree on the ability to generate, integrate and interpret high-dimensional data from preclinical model or patient samples. As such, there is increased demand for platforms enabling highly multiplexed protein and RNA analysis that preserve spatial positioning within tissue architecture. The development of multiplexed IHC greater than five markers has largely been restricted by the spectral overlap of available fluorophores or chromogens. However, multiple platforms claiming capability of multiplexing more than 20 markers have been developed in recent years, circumventing the limitations of IHC by conjugating novel species to primary antibodies and detecting them using innovative detector systems. Methods of mass cytometric detection of elemental metals conjugated to primary antibodies liberated either by UV laser [10,11] or primary ion beam [12] have been described. These methods have elucidated temporal and spatial dynamics of PD-1, PDL1 and IDO1 expression on immune cell subsets in triple-negative breast cancer [13] as well as demonstrated the ability to characterize mRNA and

protein targets in formalin-fixed, paraffin-embedded (FFPE) tissue samples [14].

Platforms capable of highly multiplexed IHC are developing rapidly, but highly multiplexed *in situ* hybridization remains challenging. A platform claiming capability of highly multiplexed protein IHC and *in situ* hybridization has been introduced by NanoString; the digital spatial profiling (DSP) platform (NanoString Technologies, Seattle, WA, USA) theoretically enables multiplexed detection of up to 800 targets simultaneously. Target-specific barcodes attached via a UV-cleavable linker to either primary antibodies or nucleic acid probes are liberated by a UV laser from user-selected regions of interest (ROI) in a tissue sample and counted using the nCounter platform. Counts are mapped back to tissue location, thus allowing spatial designation of target abundance at the resolution of the defined ROI. The precision of the UV laser reportedly allows interrogation of protein or RNA expression by single cells or can be applied to defined masks that capture a visually demarcated tissue section.

Such capabilities hold great promise in advancing tissue-based basic and translational research. However, aspects of the DSP chemistry and function require careful consideration to inform experimental design and appropriate interpretation of results. We will review the function and capabilities of the NanoString DSP platform based on the authors' research and experience. More specifically, we will present the chemistry of oligo capture and antibody-oligo conjugation as it relates to DSP, summarizing existing published work, with consideration for how samples can be interrogated with DSP and how data are produced and analyzed. These aspects will then be considered in the context of other high-level multiplexing platforms with consideration given to both preanalytical (e.g. sample quality) and analytical (e.g. ROI selection) issues to help inform sample selection, experimental design and interpretation.

From bulk RNA quantification to multiplex IHC and *in situ* hybridization

Over the past 10 years, the NanoString nCounter technology has been broadly used for mRNA, miRNA and protein quantification in bulk samples (cell or tissue lysates) in multiple fields of life science. Most recently it has been implemented in the DSP platform and its chemistry is briefly reviewed before a more detailed consideration of the principles and challenges of DSP.

NanoString nCounter principles and instrumentation

The chemistry underlying NanoString is a solution-phase hybridization reaction in which RNA targets of interest in solution are each captured by a complementary nucleic acid probe with a unique fluorescent 'barcode' and then enumerated. This is accomplished in three steps: (1) hybridization, (2) purification and immobilization, (3) counting and analysis (Figure 1). During hybridization, a population of RNA is mixed with capture and reporter probes in solution. Probes are specific to a transcript of interest and a unique labeled RNA fragment ('barcode') allows indexing of individual transcripts. Following hybridization, probe–target complexes are bound to the surface of a cartridge and are immobilized. A digital analyzer images up to several hundred fields of view (FOV) per flow cell, enumerating hundreds of thousands of barcodes. Images are then processed and the results are exported as a comma separated values (CSV) files.

It is important to note that amplification is not part of the nCounter chemistry. This is a distinguishing aspect of the platform and serves to avoid transcript-specific or 3′-amplification bias in target identification. However, concerns over its ability to detect low abundance targets may arise. Sensitivity of the platform has been demonstrated down to 0.1–0.5 fM RNA target [15]. Additional experiments have also documented the platform reproducibility ($R^2 = 0.99$ [15], $R^2 > 0.98$ [16]) and minimal impact of technical variations (probe library stability, cartridge stability, cartridge lane) on sample counts [16].

Probe barcoding: adaptation of NanoString for quantitative IHC

Driven by growing interest in tumor heterogeneity and rare cell subsets (e.g. circulating tumor cells), a highly sensitive method capable of profiling a few or even single cells with high-level multiplexing has been of increasing interest. DNA barcoding had been developed and applied to soluble proteins [17–22]. However, the application to single cells or cell suspensions was limited due to complexities of detection and barcode amplification in a cellular microenvironment. These limitations were initially surpassed by development of light-mediated cellular barcoding (LMCB). Agasti *et al* [23] developed an antibody-based proteomic profiling method that allowed the detection of proteins in live cell suspensions by antibodies conjugated to unique DNA oligomers via a UV-cleavable linker. Experiments demonstrated linear correlation of oligos liberated from anti-HER2 antibody to fluorescence-activated cell sorting (FACS)-based quantification of SK-BR3, 3T3 and MDA-MB-231 cells. Proof of concept experiments showing the detection of single SK-BR3 cells in dilution experiments and the detection of EGFR, EpCAM and HER2/neu in multiplex staining of breast cancer cell lines were also reported.

Although LMCB was a significant advance, the method was semiquantitative and PCR amplification of liberated oligos limited multiplexing to five targets and introduced 3′- and size-amplification biases. LMCB was subsequently modified by capturing liberated oligos with NanoString probe sets [24]. Liberated oligos could then be detected by the nCounter platform, eliminating the need for PCR amplification and semiquantitative

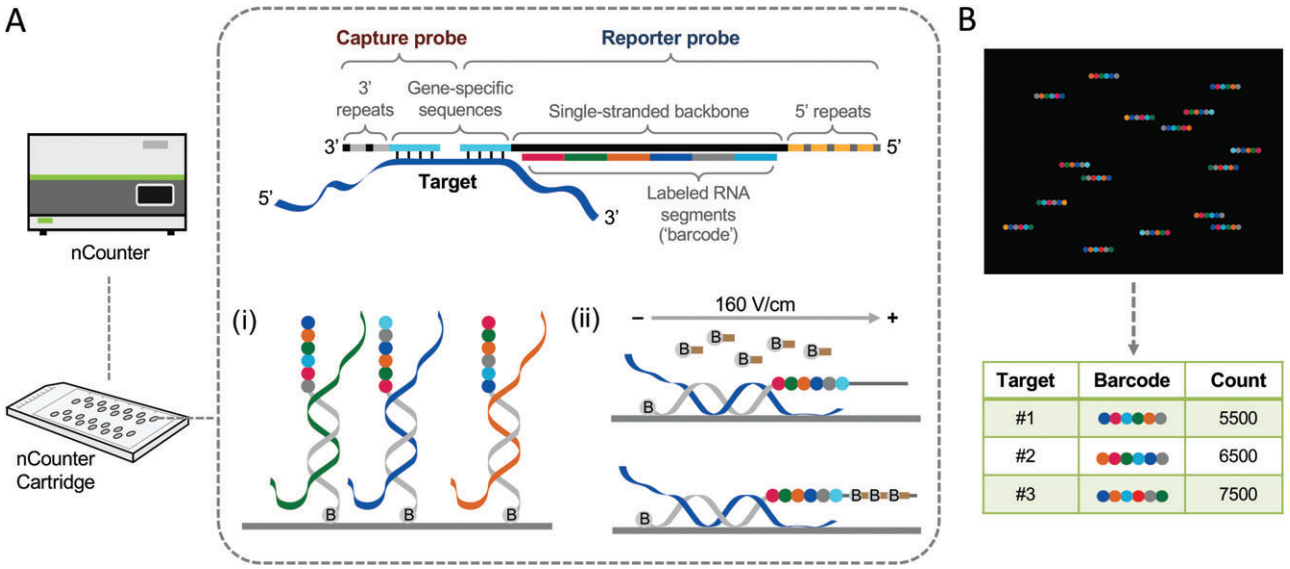

Figure 1. NanoString capture chemistry. Targets of interest in solution are captured by complementary nucleic acid probes labeled with unique fluorescent barcode and then enumerated. This is accomplished in three steps: hybridization, purification and immobilization, counting and analysis. (A) During hybridization, target RNA is mixed with capture and reporter probes. The capture probe is composed of a 35–50-base target-specific sequence attached to an oligonucleotide comprised of two 15-base, 3′ repeats linked to a biotin molecule. The reporter probe consists of a linearized, single-stranded DNA backbone annealed to six fluorescently labeled RNA segments (barcode). (i) During purification and immobilization, excess probes are removed and the probe–target complexes are bound by streptavidin coating the surface of the nCounter cartridge. (ii) Reporter probes are then stretched and aligned by applying 160 V/cm current along the fluidic channel. Stretched reporters can then be immobilized along the cartridge surface by addition of a biotinylated oligonucleotide complementary to the 5′ repeats present on the reporter probes (ii). (B) After immobilization, expression levels of transcripts are measured by imaging several hundred FOV. Barcodes present in each image are then counted and associated to their respective target. Figure adapted from [15].

gel readout. Proteomic profiling experiments demonstrated detection of up to 90 proteins in fresh/frozen core biopsy samples. Validation work further demonstrated comparable performance between conjugated and unconjugated antibodies, reproducibility, identical staining of markers alone and as part of a 60-member cocktail and high correlation ($R^2 = 0.92–0.99$) of expression of six markers (CD44, HER2, EGFR, CA19-9, CK7, MUC1) to flow cytometry.

The principles and instrumentation of NanoString DSP technology

The antibody conjugation method was subsequently adopted by NanoString, who developed a specialized microscope for interrogation of tissue samples and subsequent analysis on the nCounter platform. Once sample selection and experimental design are set, the workflow can be broadly divided into three general components: (1) sample staining and imaging, (2) ROI selection, (3) collection and analysis (Figure 2).

Sample considerations and experimental design

DSP can interrogate fresh frozen or FFPE samples with validated panels targeting up to 40 protein or over 90 RNA targets. Preanalytical variables have significant impact on protein and RNA quality for both sample types and have been examined extensively [25,26]. Although mandatory requirements for DSP processing are not defined, it is suggested that for RNA analysis FFPE samples be less than 4 years old and fixed in 10% neutral buffered formalin for more than 16 h. Pilot studies conducted by our laboratory using samples less than 3 years old and with cold ischemic times less than 15 min showed robust detection of the 40 protein targets and good RNA target detection, the quality of detection being sample-, ROI- and target-dependent for the latter.

For protein targets, cold ischemic times [27,28], fixation duration [29–31] and specimen age [32] have documented effects on IHC quality. Although archival tissue blocks are suitable for DSP analysis, the standardization of sample collection, fixation and processing is recommended where possible for prospective studies. As this is usually not possible for archival FFPE samples, markers correlated to cold ischemic time have been demonstrated [33,34] and their inclusion into a multiplex panel is a possible tissue quality control.

Sample staining and imaging

In the current workflow, IHC or *in situ* hybridization are performed on separate slides. Slides are first subjected to a 'one-size-fits-all' pH 6.0 citrate antigen retrieval for IHC or proteinase K digestion for *in situ* hybridization. In both cases, slides are also stained with fluorescently labeled antibodies (three or four markers) chosen by the user to visualize tissues or cells of interest and guide ROI selection. For example, panCK, CD3, CD20 and DAPI, each conjugated to a different fluorophore, might be used to visualize and select tumor, T cell-rich

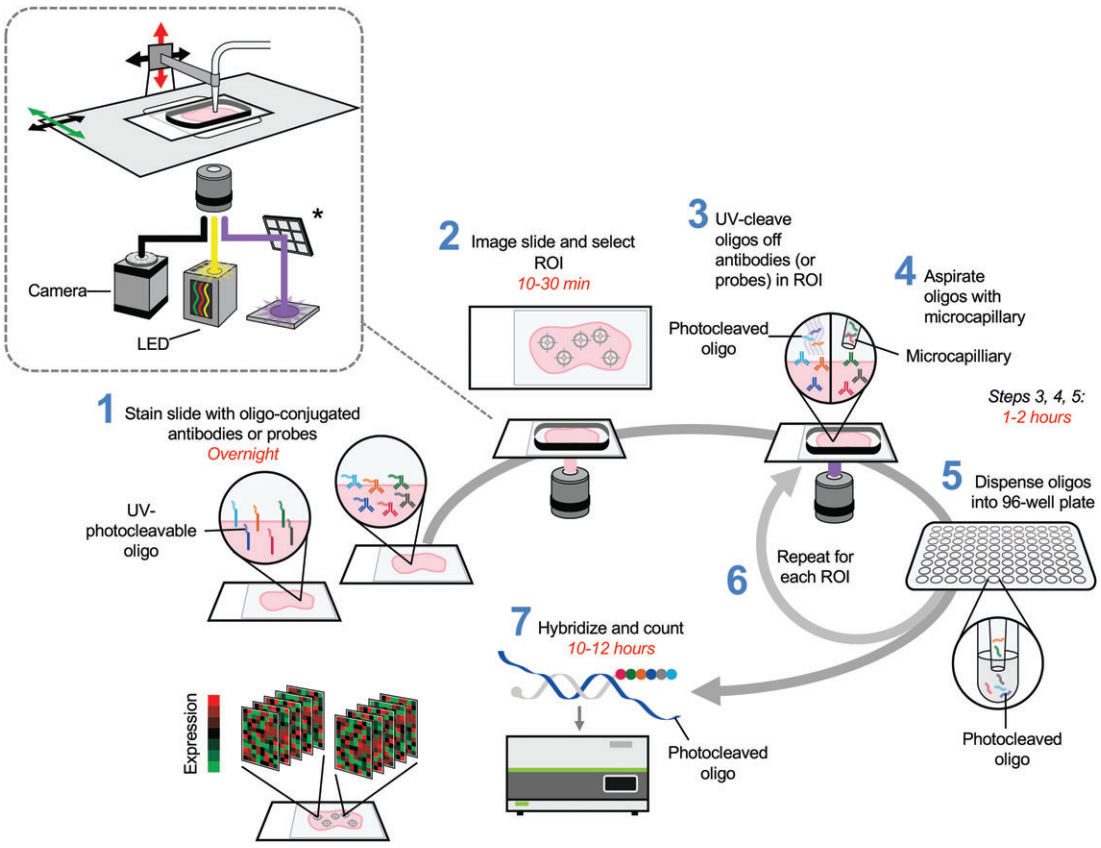

Figure 2. Workflow for the NanoString DSP platform. (1) Separate slides stained either with an antibody cocktail or used for hybridization with an RNA probe. Slides are also stained with a small panel of fluorescently labeled antibodies for tissue visualization. (2) Slides are placed on a mobile microscope stage. Tissue is visualized on the DSP microscope using fluorescent antibodies. Overlying the sample slide is a buffer-filled gasket and microcapillary sipper mobile in the XZ plane for probe collection. The imaged slide can be used to select ROI, which will guide application of the UV laser (*). (3) UV illumination of selected ROI liberates the attached oligos from antibodies or RNA probes. (4) Oligos are collected by the microcapillary and (5) deposited into a well of a 96-well plate. (6) The process is then repeated for the next ROI. (7) Positive and negative control ERCC probes are introduced. Liberated oligos and controls are hybridized to capture and reporter probes and counted by the nCounter. Figure adapted from NanoString, Inc (https://www.nanostring.com/scientific-content/technology-overview/digital-spatial-profiling-technology, last accessed 1 October 2018).

or B cell-rich ROI from a lung carcinoma sample. For multiplexed IHC, these visualization markers are incorporated into a cocktail of oligo-tagged antibodies. For *in situ* hybridization, tissue slides are prepared by standard protocols, incubated with a RNA detection probe cocktail, then stained with fluorescently labeled antibodies for tissue visualization. Positive and negative antibody and RNA transcript controls are incorporated into the respective cocktails. Slides are stained overnight, mounted on a microscope stage and wide-field epi-fluorescence imaging is then performed to create a digital image from which ROI will be designated.

Although RNA and protein analyses are performed on separate slides, it is advisable to use consecutive tissue sections to allow correlation of RNA and protein data. With average section thickness being 3–4 μm, this will allow preservation of overall tissue architecture and minimize variability between RNA and protein datasets. Single-cell protein and RNA analyses could not be correlated between serial sections due to section thickness. However, it is theoretically possible to identify single cells using the limited panel of fluorescent antibodies that is part of *in situ* hybridization on the DSP if appropriate visualization markers are chosen.

Region selection

Although a whole-slide image is created for reference using fluorescent visualization markers, DSP interrogates only smaller, user-defined regions. These ROI are selected and digitally placed onto the whole-slide image. These ROI are then UV illuminated and the liberated oligos are collected. Three types of ROI are possible on the DSP platform: (1) 'geometric', (2) 'phenotypic' and (3) single cell (Figure 3). A geometric ROI is represented either as a rectangle (up to 600 × 600 μm) or circle (100–650 μm diameter) and the UV laser illuminates the entire ROI. Phenotypic ROI are more restrictive and can be generated from a fluorescent marker incorporated into the staining cocktail. For example, TTF-1 staining of a non-small cell lung carcinoma sample will highlight tumor cells. A ROI overlying only the stained cells can then be generated by the image analysis software. The UV laser then illuminates these ROI(s), enabling a cell-type or compartment-specific interrogation of the tissue. Similarly, single-cell ROI can be generated by

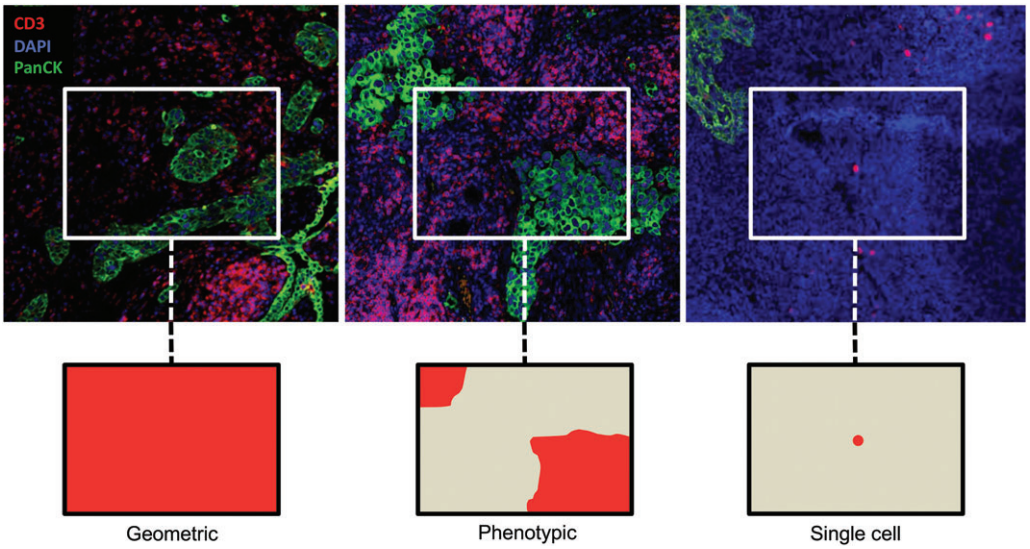

Figure 3. ROI types. Three types of region can be interrogated by DSP. Selected ROI (in red on schematics) are illuminated by a UV beam liberating oligos from antibodies or RNA probes only within that region. Geometric ROI can be selected as rectangles from 100 × 100 µm up to 600 × 600 µm or circles up to 650 µm in diameter. Phenotypic ROI are generated based on marker expression and can restrict interrogation to only tumor cells or stroma. Single-cell ROI are generated based on marker expression and allow interrogation of either one or multiple single cells within a FOV.

overlay of an ROI onto fluorescent single cells within a FOV. The UV laser can then be focused as narrow as 10 µm in diameter to illuminate a single cell within the field.

Collection and analysis

Following illumination of an ROI, the oligos conjugated to the antibodies present are liberated into the buffer within the gasket overlying the tissue. A microtiter pipette ('sipper') aspirates and dispenses the oligos into a well of a 96-well plate for processing on the nCounter platform. The process is then repeated for the next ROI. For the case of geometric ROI, each ROI is ultimately deposited into a separate well in the plate. However, it should be noted in the phenotypic ROI example above that the TTF-1-positive compartment of the entire tissue sample is not interrogated. It occurs only in restricted FOV (600 × 600 µm) selected by the user. The phenotypic mask from each FOV is deposited into a separate well. For single-cell masks, the case is similar: oligos from all interrogated single cells within a FOV are typically collected and deposited into a plate well together. It is possible to analyze single cells (one cell per well) but sampling and analyzing sufficient numbers can be cost-prohibitive.

Following deposition of aspirates, the plate is placed in the preparation station and the NanoString probe set is introduced. Each RNA or antibody-specific oligo is thus coupled to a reporter probe with a unique barcode allowing discrimination and enumeration of all bound antibodies within a given ROI on the nCounter. During analysis, External RNA Control Consortium (ERCC)-positive and -negative control transcripts are included to normalize for technical variables such as hybridization efficiency. Antibody and RNA counts, control probe counts and normalization calculations are compiled for analysis.

Importantly, the DSP does not allow for an image reconstruction of the interrogated sample. The only spatial information associated with the targets is the ROI from which they were collected. Thus, probing multiple ROI with one tissue section is an alternative approach to assess a sample's heterogeneity.

DSP capabilities and validation

The chemical and technical complexity of the DSP platform suggests the need for robust validation of its technical performance, sensitivity and reproducibility. Both NanoString and third parties have performed some of these experiments and published results are briefly summarized here. To establish the limit of detection for antibody staining, an approach measuring CD3, CD45 or PD1 nCounter counts from increasing, concentric UV-illuminated areas of tonsil (100–1000 µm diameter) or CCRF-FEM T-ALL cell pellets (50–650 µm) has documented linearity ($R^2 = 0.98–0.99$) over 5 logs down to approximately 25 µm resolution (one to four cells) [35,36]. Similarly, the diameter and positional accuracy of the UV beam has also been explored and the linearity ($R^2 = 0.984$) of one-, two-, four- and eight-cell ROI has been demonstrated [35]. Although prior experiments examined the efficiency of UV-mediated oligo cleavage and found near complete cleavage after 15 min of exposure [24], additional experiments on the DSP have demonstrated that 5 s of irradiation gives near complete cleavage of oligos linked to CD45, CD31 and histone (personal communication). High technical reproducibility for HER2 quantification [37] as well as

other targets has also been demonstrated. Serial tissue sections were stained and analyzed with a 29-protein target panel 1 month apart and counts for 24 ROI per sample were compared for each marker. Twenty-one of 29 markers showed $0.69 < R^2 < 0.92$, seven of 29 showed $0.51 < R^2 < 0.69$ and one (Foxp3) showed poor correlation ($R^2 = 0.40$) [38].

Validation of DSP quantitation against established methods such as flow cytometry and traditional IHC has also been demonstrated. Detection of HER2 with the DSP platform has shown high correlation ($R^2 = 0.92$) to pixel intensity of fluorescence staining [36] as well as automated quantitative immunofluorescence [37]. DSP quantitation of CD3, CD4, CD20, CD56, CD45RO and CD8 has also shown good correlation ($R^2 = 0.65$) to flow cytometry cell counts in a peripheral blood mononuclear cell pellet [38]. A correlation to cell counts by IHC in tonsil has been shown for multiple markers, including CD3 ($R^2 = 0.80$), CD4 ($R^2 = 0.66$), PD-1 ($R^2 = 0.74$) and CD8 ($R^2 = 0.75$) [39]. Correlation to CD3 ($R^2 = 0.72$), CD4 ($R^2 = 0.80$) and CD45 ($R^2 = 0.90$) cell area has also been demonstrated from serial lung sections [38]. It should be noted that although correlation for such abundant markers is strong, correlation for low abundance markers, such as granzyme B, Foxp3, PD-1 and PDL1, has appeared less robust in tumor tissues [38]. To a large extent, this probably represents performance differences between clones used in the respective assays as well as exaggerated section-to-section variability for low-abundance populations. Application of the DSP technology to tissue RNA analysis has shown robust detection of RNA in both frozen and FFPE samples as well as good correlation with RNAscope analysis [40]. However, additional RNA analysis validation data have not been publicly presented at the time of writing.

DSP data evaluation and analysis

In order to evaluate the DSP performance, we conducted a pilot study on three non-small cell lung cancer FFPE samples (Figure 4A), analyzing 32 protein and 82 RNA targets in 24 ROI, split equally between tumor and stromal regions of each specimen. Protein and RNA panels were conducted on non-serial tissue sections and data were analyzed in parallel. The DSP generates high-dimensional data that can introduce significant variance, complicating results interpretation. We identified four sources of variance (Figure 4A), either technical or biological. First, probe quantification in the nCounter can be a source of technical variance. As introduced above, ERCC probes are added to the samples before quantification to normalize for quantification efficacy. This method has been routinely used for conventional RNA quantification, thus only ERCC-corrected counts should be used for further analysis of DSP data. Second, to adapt to tissue architecture, ROI may differ in size across one sample, which may impact the overall signal coming from each area. In order to compare ERCC-corrected counts, area normalization should be applied. Third, the major variable introduced by the DSP is the direct interrogation of tissues. Classical RNA quantification on bulk cells or tissues needs to be normalized for cellular content and thus relies on the presence of reference transcripts within samples for normalization. In the DSP, tissue heterogeneity needs to be considered, as different regions will differ in background and cellularity. Moreover, although the presence of RNA transcript mainly relies on the presence of cells, this is less true for proteins that can be secreted and released in the extracellular milieu. The DSP has incorporated solutions to these issues. To control for ROI background, eight negative probes are included in the RNA panel and two isotype antibodies (mouse IgG2a and rabbit IgG) are part of the protein panel. To control for cellularity, four reference transcripts (*UBB*, *OAZ1*, *SDHA*, *POLR2A*) and two antibodies against cellular proteins (Histone H3, ribosomal protein S6) are included in the RNA and protein panels, respectively.

We evaluated how background and cellularity varied between stromal and tumor ROI (Figure 4B). To assess background, RNA-negative probes (not specific for any human transcripts) were used. As shown in one representative sample, RNA-negative probes showed an overall increased signal in stromal areas, whereas reference transcript counts were in the same range. In the protein panel, tumor ROI showed increased signal with isotype antibodies, whereas reference proteins were comparable. These variations in background and cellularity in tissue regions, observed to a various degree in the three samples, indicate that tissues are not homogeneous and that normalization for either background or cellularity will lead to different observations.

Once ERCC-corrected counts are obtained, both RNA and protein panels can be normalized for background (signal to noise ratio; SNR) or cellularity (reference normalization; RN) as detailed in Figure 4C. We aimed to compare how these two normalization methods influence data interpretation. We explored how transcript and protein signatures differ between tumor and stromal ROI using either SNR or RN datasets. For each sample, we compared the clustered ROI types against each other and looked at the markers that were significantly different between region types. The Venn diagrams show the numbers of markers that are significantly different between the types of area and how the normalization method influences this number. Taking sample 043667T2 as an example, we observed that 44 RNA and 23 proteins were differentially expressed between tumor and stromal ROI using SNR, whereas these numbers were 54 RNA and 27 proteins using RN. Moreover, three RNA and one protein were statistically significant only with SNR, whereas 13 RNA and five proteins were only significant using RN. These variations between normalization methods were observed in all three samples. This highlights the complexity in data normalization and the need for a careful and consistent approach when analyzing DSP results.

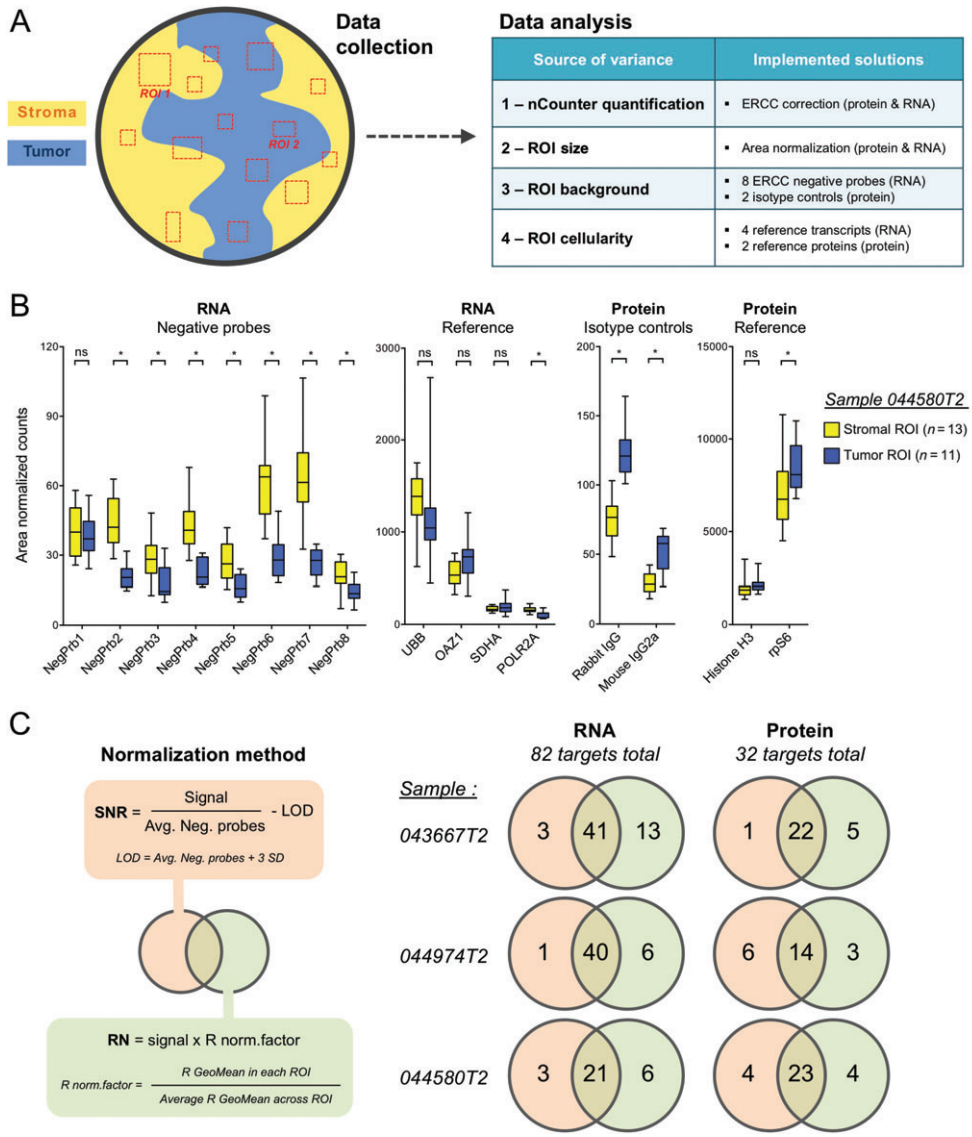

Figure 4. DSP pilot study – analysis workflow and data evaluation. (A) Schematic of the pilot study designed to assess NanoString DSP performance in three non-small cell lung cancer FFPE samples. Tumor and stromal ROI (11 – 12 of each) were selected in each specimen based on their pathological features on fluorescent visualization markers, CD3, panCK and DAPI. Selected ROI were applied on consecutive sections for DSP analysis. Once data are collected, DSP users need to be aware of the normalization parameters that allow ROI comparison within and across samples as presented in the table. (B) Area normalized counts of control and reference probes are shown for the RNA and protein panels in one representative sample. Counts were compared between stromal and tumor ROI to highlight the influence of architectural heterogeneity within a tissue. *t*-test corrected for multiple testing was used for statistical analysis, $*q < 0.05$. (C) Protein and RNA datasets normalized with SNR (orange circles) or RN (green circles) methods were used to compare the RNA and protein signatures of tumor and stromal ROI. Detailed normalization formulas are indicated on the left. Each circle shows the number of markers significantly different between tumor and stromal ROI. Venn diagrams are used to show differences and similarities when comparing the two normalization methods. FDR-adjusted p values ($q < 0.05$) were used as the cut-off for statistical significance.

Although there is no correct answer on how to best normalize the DSP data, in our experience SNR appears to be the most appropriate, as it will discard non-biological variance. Normalization to reference targets can control for regional differences in cellularity; however, this would not be applicable to experiments interrogating such differences, e.g. T cell prevalence in tumor versus stromal regions. Thus, we recommend adapting the normalization methods to each experiment, which will be influenced by the degree of the complexity of the tissues analyzed and the question asked.

Single-cell analysis

Single-cell analysis has enhanced the characterization of cancer heterogeneity [41–45], improved mechanistic insights into cancer progression and may ultimately aid the evolution of cancer classification and the development of novel strategies for both chemo- and immunotherapies [46–52]. Additionally, the impact of even rare immune cell subsets on tumor progression and prognosis has been demonstrated [53–56]. The DSP has demonstrated an ability to interrogate very few or single cells and is a potentially powerful tool for such studies.

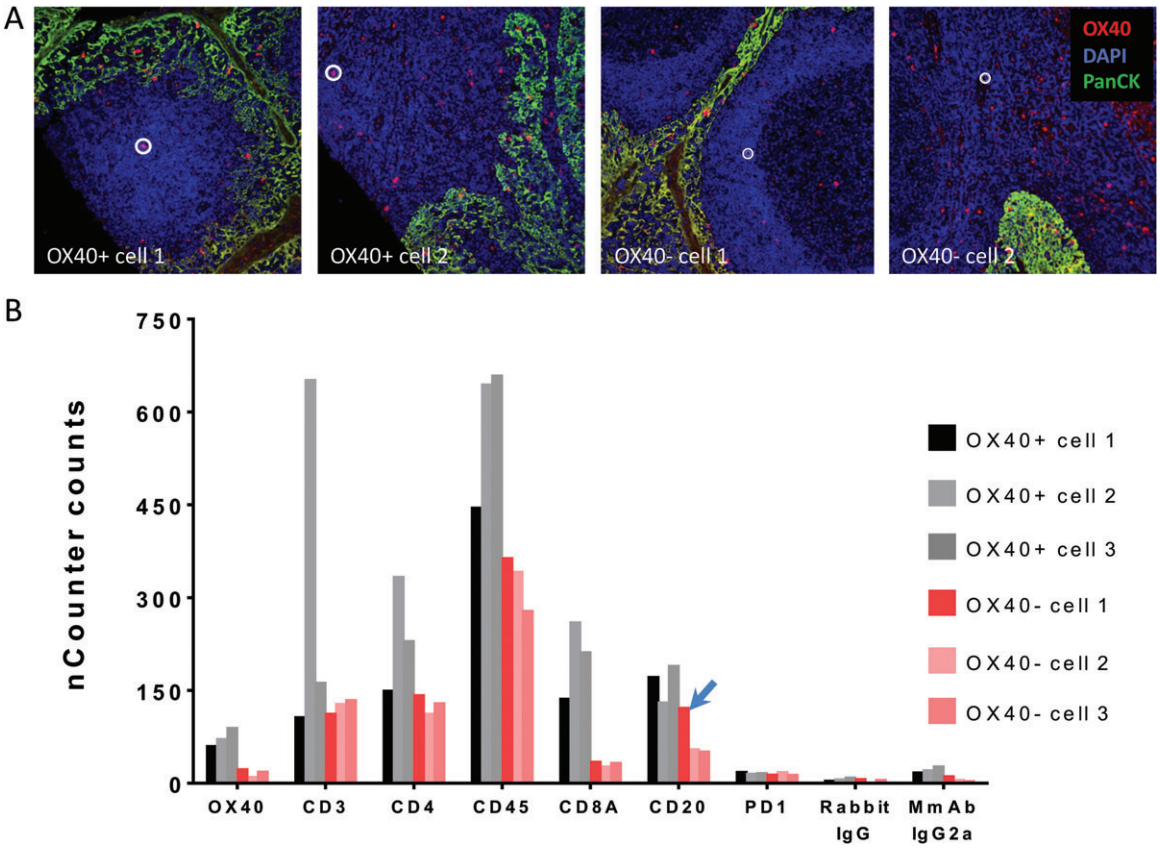

Figure 5. Single-cell analysis of OX40-positive and OX40-negative cells by DSP. (A) Analysis on single cells requires selection of OX40-positive and -negative single-cell ROI using fluorescent OX40 staining for visualization. (B) nCounter counts from OX40-negative ROI establish background levels of OX40 staining and isotype controls establish general background staining levels. Counts above these levels may be considered 'positive' expression (or an arbitrary greater threshold set). By these criteria, surface marker expression for single cells appears anomalous and probably reflects collection of two or several adjacent cells. Counts for other markers vary significantly and 'negative' ROI may not be negative for markers of interest, e.g. CD20 (arrow).

However, such data must be carefully interpreted and considered in light of certain technical limitations.

For many markers, visual interpretation of expression by standard IHC is binary (positive/negative). However, oligo tags counted by the DSP platform are continuous. To assign cell identity, a threshold must be set to define 'positive' and 'negative.' For single cells, this can be accomplished by selecting certain 'negative' regions of tissue, e.g. connective tissue or individual cells negative for a marker of interest, to establish a background level of staining.

However, pilot studies conducted in our laboratory suggest that data can still be difficult to interpret. For example, marker counts for three individual OX40-positive cells stained in a tonsil sample are somewhat unexpected (Figure 5). Cell 1 is OX40/CD8/CD20/CD45-positive, cell 2 is OX40/CD3/CD4/CD20/CD45-positive and cell 3 is OX40/CD4/CD45/CD8/CD20-positive. Although OX40 expression on CD4 [57,58] and CD8 T cells [59,60] is known and expression on B cells, dendritic cells and eosinophils has been suggested [61], the observed phenotypes are anomalous. Overlap of the UV beam between adjacent B and T cells may explain this pattern. However, this is recognizable due to the known expression pattern of these markers. If novel markers were being interrogated, establishing definitive expression profiles for each cell would be difficult. These issues would probably be resolved in analyses of large numbers of OX40-positive cells. However, the discrimination and characterization of single or small numbers of immune cell subsets could be challenging and samples as well as ROI must be carefully selected to optimize such an analysis.

NanoString DSP and other multiplexing methods

Apart from NanoString, several technologies currently enable high-level multiplex immunostaining of FFPE tissues and are at varying stages of technical and commercial maturity. Although all achieve multiplexing of more than 20 protein markers, none have demonstrated highly multiplexed RNA target detection, their capabilities differ and access to the technology can be limited and/or costly. Also, significant computational expertise in image analysis is often necessary to interpret the results. As such, potential users must carefully consider their experimental question(s) and needs in the context of the various platforms' capabilities. We briefly summarize here the current capabilities of mass spectrometry (MS)-based platforms and cyclic multiplex staining methods and consider NanoString DSP in their context.

Secondary ion MS has been incorporated into two platforms to image antibodies tagged with isotopically pure elemental metals in FFPE tissues. The first couples laser ablation with CyTOF and is commercially available as the Hyperion Imaging System (Fluidigm Corp., South San Francisco, CA, USA) for imaging mass cytometry (IMC). In IMC, following antigen retrieval, FFPE tissue is stained with a cocktail of antibodies, each conjugated to a specific rare earth isotope. ROI are selected from an unstained, digitized whole-slide image and each region is rasterized with a pulsed laser (1 μm^2 spot) and the liberated ions are introduced into the inductively coupled plasma time-of-flight (TOF) MS. The ion counts for each pulse can then be assembled into a protein expression image for each ROI with a resolution of 1 μm^2.

The principle of multiplexed ion beam imaging (MIBI) is similar but with several distinct features. MIBI uses a custom-designed TOF MS equipped with a duoplasmatron primary O_2+ ion source rather than a laser. Also, tissues must be mounted on tantalum and gold-coated, conductive slides. ROI are selected from a digitized whole-slide image and corresponding positions on the tissue are sequentially sputtered with the O_2+ primary ion beam at 500 nm probe size/resolution. Secondary ions are collected and pass through an orthogonal TOF MS. Events are then recorded and TOF spectra for each pixel are summed and saved to a data file.

By contrast to these platforms, MultiOmyx (Neogenomics, Fort Myers, FL, USA) uses a cyclic staining approach. Three to four fluorescently labeled antibodies are applied to a tissue, ROI (700×700 µm) are imaged, fluorophores are chemically quenched with an alkaline solution and the cycle repeats with a new antibody cocktail. Subsequent imaging steps require microscopic realignment of ROI on the tissue. Images taken for each round can then be co-registered by DAPI staining and pseudo-colored, multiplexed images generated.

The platforms, including DSP, share several features (Table 1). Each interrogates only small ROI, which together could fully characterize core biopsy samples but constitute only a minor fraction of an average excisional biopsy specimen. Also, each must subject the sample tissue to a 'one-size-fits-all' antigen retrieval process that may not be optimal for multiple antibodies in the staining panel, resulting in either decreased sensitivity or significant background staining. The platforms also employ primary conjugated antibodies. As such, with the exception of MultiOmyx, amplification cannot be introduced.

Unlike IMC, MIBI and cyclic staining methods, a unique feature of DSP is that apart from fluorescent antibodies used for ROI selection, targets cannot be visualized. Although highly multiplexed images can be generated via IMC or MIBI through assignment of ion counts to individual pixels or via MultiOmyx through co-registration of images, oligos cannot be assigned to individual pixels to reconstruct a tissue image on DSP. Markers are only detected as counts in the predefined ROI. This facilitates data management by eliminating the need for image analysis [63–65]. However, the drawback of such an approach is that visual verification of staining quality and specificity is not possible. Spatial information, such as distances between immune cell subsets, can have prognostic relevance [66] and such analyses of larger numbers of immune cell subsets could be even more informative. However, analysis of such morphological features by DSP would at least require careful planning of visualization markers and ROI selection but seems largely restricted as the majority of targets cannot be visualized.

Conclusion and perspective

The NanoString DSP offers great opportunities to interrogate tissue samples at a high-dimensional level and it should be noted that the platform is rapidly evolving and many of its technical aspects may have changed or improved even by the time of writing. Two recent studies have used NanoString DSP to characterize the tumor protein profile of melanoma patients receiving immune checkpoint blockade therapy and showed that baseline immune infiltration was correlated with treatment efficacy [67,68].

Validation work performed by our laboratory and others' have demonstrated robust detection of high abundance protein and RNA targets, dynamic range significantly greater than traditional IHC and good to excellent reproducibility and correlation to gold standard methods. Although these attributes can generate unprecedented data from archival tissue samples, aspects of the method must be carefully considered when designing experiments and interpreting results. For instance, single-cell analyses typically aggregate oligos from multiple individual cells in a plate well, allowing analysis of associations between markers, e.g. CD3, CD4 and CD8. However, the amount of individual CD3 + CD4-positive versus CD3 + CD8-positive cells cannot be enumerated. Single cells (one cell per well) can be interrogated but defining 'positive' expression for any given protein marker requires consideration of background levels. These can be established via the included isotype controls and/or consideration of counts from a 'negative' region of tissue for a given marker. Although these are helpful methods to determine true expression, establishing a threshold remains arbitrary. In addition, tissue areas 'negative' for certain markers may not be present or distinguishable in certain sample types or tissues. As such, both tissue and ROI selection must be carefully considered in designing an experiment.

Data normalization is an important and dynamic question in analyzing multidimensional datasets, and no clear solutions can be given. Although NanoString RNA quantification has been around for more than 10 years, normalization methods are still being optimized [69]. One must be aware of the pitfalls inherent to each technology and samples analyzed and integrate these

Table 1. Features of high multiplexing (>20 targets) platforms

	DSP (NanoString)	IMC (Fluidigm)	MIBI (IonPath)	MultiOmyx (GE)
Species detected	Protein and RNA	Protein and RNA	Protein and RNA	Protein and RNA
Detected reporter	Nucleic acid 'barcode'	Lanthanide metal ions	Lanthanide metal ions	Fluorophore
Maximum plex Theoretical	800	>50	>50	Infinite
Maximum plex Published	32 proteins, 82 RNA [38]	32 proteins [11] 16 proteins, 3 RNA [14]	36 proteins [13]	61 proteins [62]
ROI size	User-defined Up to 600 × 600 µm	User-defined	User-defined	600 × 700 µm
Speed of acquisition	30 min per slide (20–40 ROI)	30 min (500 × 500 µm)	18 min (500 × 500 µm)	5–10 min per ROI (700 × 700 µm)
Resolution	10 µm	1 µm	200 nm	1 µm
Number of markers visible	3–4 (visualization markers)	All	All	All

parameters in their analysis. Working in collaboration with computational scientists is essential in order to maximize the quality of the data generated. Although this was not assessed in our pilot studies, detection of fusion or splice variants could also be performed using this platform.

For DSP experiments, it is also important to consider that the antibody conjugation chemistry is not a site-specific reaction with tightly controlled stoichiometry. In fact, the number of oligos per antibody appears highly heterogeneous between clones [24]. It is unknown if and how the conjugation performed by NanoString differs from the originally published method. However, normalization of results to average oligo tags per clone may be an important step in results interpretation.

In the context of translational research, the ability to explore banked samples with multiplexing platforms allows for retrospective analysis of clinical studies, for example. Other approaches are also taken in order to characterize tissue heterogeneity and complexity. In particular, single-cell RNA sequencing offers the possibility to explore this issue. Such methods have been used to reconstruct the immune landscape of breast tumor samples [70]. That said, this approach is limited to the analysis of fresh tissues with the logistic limitations implied and can only interrogate its cellular component. Thus, being able to characterize the whole tissue diversity remains important for a better understanding of pathologies.

Acknowledgements

The authors wish to thank Alison Bruce for her illustration work on the figures and Vincent Rouilly (Genentech, Inc.) for his advice on data analysis.

Author contributions statement

JZ, JD and MLA were responsible for conception and design. JZ and JD drafted the original manuscript, collected data and designed the figures.

References

1. Allred CD, Carlson RW, Berry DA, *et al.* NCCN task force report: estrogen receptor and progesterone receptor testing in breast cancer by immunohistochemistry. *J Natl Compr Canc Netw* 2009; **7**(Suppl 6): S1–S21.
2. Khoury JD, Wang W-L, Prieto VG, *et al.* Validation of immunohistochemical assays for integral biomarkers in the NCI-MATCH EAY131 clinical trial. *Clin Cancer Res* 2018; **24:** 521–531.
3. Mohsin SK, Weiss H, Havighurst T, *et al.* Progesterone receptor by immunohistochemistry and clinical outcome in breast cancer: a validation study. *Mod Pathol* 2004; **17:** 1545–1554.
4. Farzin M, Sioson L, Clarkson A, *et al.* Immunohistochemistry first as a screening strategy for targeted therapy of lung cancer. *Pathology* 2012; **44:** S76–S77.
5. Sanmamed MF, Chen L. A paradigm shift in cancer immunotherapy: from enhancement to normalization. *Cell* 2018; **175:** 313–326.
6. Colak S, Medema JP. Human colonic fibroblasts regulate stemness and chemotherapy resistance of colon cancer stem cells. *Cell Cycle* 2016; **15:** 1531–1537.
7. Baker JHE, Kyle AH, Reinsberg SA, *et al.* Heterogeneous distribution of trastuzumab in HER2-positive xenografts and metastases: role of the tumor microenvironment. *Clin Exp Metastasis* 2018; **19:** 1–15.
8. Chung LWK, Huang W-C, Sung S-Y, *et al.* Stromal–epithelial interaction in prostate cancer progression. *Clin Genitourin Cancer* 2006; **5:** 162–170.
9. Chen DS, Mellman I. Elements of cancer immunity and the cancer–immune set point. *Nature* 2017; **541:** 321–330.
10. Bodenmiller B. Multiplexed epitope-based tissue imaging for discovery and healthcare applications. *Cell Syst* 2016; **2:** 225–238.
11. Giesen C, Wang HAO, Schapiro D, *et al.* Highly multiplexed imaging of tumor tissues with subcellular resolution by mass cytometry. *Nat Methods* 2014; **11:** 417–422.
12. Angelo M, Bendall SC, Finck R, *et al.* Multiplexed ion beam imaging of human breast tumors. *Nat Med* 2014; **20:** 436–442.
13. Keren L, Bosse M, Marquez D, *et al.* A structured tumor–immune microenvironment in triple negative breast cancer revealed by multiplexed ion beam imaging. *Cell* 2018; **174:** 1373–1387.
14. Schulz D, Zanotelli VRT, Fischer JR, *et al.* Simultaneous multiplexed imaging of mRNA and proteins with subcellular resolution in breast cancer tissue samples by mass cytometry. *Cell Syst* 2018; **6:** 531.
15. Geiss GK, Bumgarner RE, Birditt B, *et al.* Direct multiplexed measurement of gene expression with color-coded probe pairs. *Nat Biotechnol* 2008; **26:** 317–325.
16. Veldman-Jones MH, Brant R, Rooney C, *et al.* Evaluating robustness and sensitivity of the NanoString technologies nCounter platform

to enable multiplexed gene expression analysis of clinical samples. *Cancer Res* 2015; **75:** 2587–2593.
17. Nam JM. Nanoparticle-based bio-bar codes for the ultrasensitive detection of proteins. *Science* 2003; **301:** 1884–1886.
18. Bao YP, Wei T-F, Lefebvre PA, *et al.* Detection of protein analytes via nanoparticle-based bio bar code technology. *Anal Chem* 2006; **78:** 2055–2059.
19. Wacker R, Ceyhan B, Alhorn P, *et al.* Magneto immuno-PCR: a novel immunoassay based on biogenic magnetosome nanoparticles. *Biochem Biophys Res Commun* 2007; **357:** 391–396.
20. Fredriksson S, Dixon W, Ji H, *et al.* Multiplexed protein detection by proximity ligation for cancer biomarker validation. *Nat Methods* 2007; **4:** 327–329.
21. Sano T, Smith CL, Cantor CR. Immuno-PCR: very sensitive antigen detection by means of specific antibody-DNA conjugates. *Science* 1992; **258:** 120–122.
22. Hendrickson ER, Truby TMH, Joerger RD, *et al.* High sensitivity multianalyte immunoassay using covalent DNA-labeled antibodies and polymerase chain reaction. *Nucleic Acids Res* 1995; **23:** 522–529.
23. Agasti SS, Liong M, Peterson VM, *et al.* Photocleavable DNA barcode–antibody conjugates allow sensitive and multiplexed protein analysis in single cells. *J Am Chem Soc* 2012; **134:** 499–502.
24. Ullal AV, Peterson V, Agasti SS, *et al.* Cancer cell profiling by barcoding allows multiplexed protein analysis in fine-needle aspirates. *Sci Transl Med* 2014; **6:** 219ra9.
25. Bass BP, Engel KB, Greytak SR, *et al.* A review of preanalytical factors affecting molecular, protein, and morphological analysis of formalin-fixed, paraffin-embedded (FFPE) tissue: how well do you know your FFPE specimen? *Arch Pathol Lab Med* 2014; **138:** 1520–1530.
26. Turashvili G, Yang W, McKinney S, *et al.* Nucleic acid quantity and quality from paraffin blocks: defining optimal fixation, processing and DNA/RNA extraction techniques. *Exp Mol Pathol* 2012; **92:** 33–43.
27. Khoury T, Sait S, Hwang H, *et al.* Delay to formalin fixation effect on breast biomarkers. *Mod Pathol* 2009; **22:** 1457–1467.
28. Bai Y, Tolles J, Cheng H, *et al.* Quantitative assessment shows loss of antigenic epitopes as a function of pre-analytic variables. *Lab Invest* 2011; **91:** 1253–1261.
29. Sathyanarayana UG, Birch C, Nagle RB, *et al.* Determination of optimum formalin fixation duration for prostate needle biopsies for immunohistochemistry and quantum dot FISH analysis. *Appl Immunohistochem Mol Morphol* 2015; **23:** 364–373.
30. Werner M, Chott A, Fabiano A, *et al.* Effect of formalin tissue fixation and processing on immunohistochemistry. *Am J Surg Pathol* 2000; **24:** 1016–1019.
31. Webster JD, Miller MA, DuSold D, *et al.* Effects of prolonged formalin fixation on diagnostic immunohistochemistry in domestic animals. *J Histochem Cytochem* 2009; **57:** 753–761.
32. Nuovo AJ, Garofalo M, Mikhail A, *et al.* The effect of aging of formalin-fixed paraffin-embedded tissues on the in situ hybridization and immunohistochemistry signals in cervical lesions. *Diagn Mol Pathol* 2013; **22:** 164–173.
33. Neumeister VM, Parisi F, England AM, *et al.* A tissue quality index: an intrinsic control for measurement of effects of preanalytical variables on FFPE tissue. *Lab Invest* 2014; **94:** 467–474.
34. Neumeister VM, Anagnostou V, Siddiqui S, *et al.* Quantitative assessment of effect of preanalytic cold ischemic time on protein expression in breast cancer tissues. *J Natl Cancer Inst* 2012; **104:** 1815–1824.
35. Merritt C, Jung J, Ong G, *et al.* Abstract 3955: spatially resolved, multiplexed digital characterization of protein and mRNA distribution and abundance in formalin-fixed, paraffin-embedded (FFPE) tissue sections based on NanoString's digital spatial profiling (DSP) technology: applications to immuno-oncology (IO) and tumor heterogeneity. *Cancer Res* 2017; **77**(13 Suppl): 3955.
36. Cesano A, Beechem J, Webster P, *et al.* Abstract 1371: spatially-resolved, multiplexed digital characterization of protein distribution and abundance in FFPE tissue sections. *Cancer Res* 2016; **76**(14 Suppl): 1371.
37. Toki MI, Merritt C, Ong G, *et al.* Abstract 3810: validation of novel high-plex protein spatial profiling quantitation based on NanoString's digital spatial profiling (DSP) technology with quantitative fluorescence (QIF). *Cancer Res* 2017; **77**(13 Suppl): 3810.
38. Ziai J, Caplazi P, Decalf J, *et al.* Abstract 2089: highly multiplexed analysis of immune cell subsets in non-small cell lung cancer: validation of protein and RNA analysis by the Nanostring digital spatial profiling (DSP) platform. *Cancer Res* 2018; **78**(13 Suppl): 2089.
39. Lee D, Liang Y, Merritt C, *et al.* A new approach for immuno-oncology biomarker discovery: high-plex, spatial protein profiling based on NanoString digital quantification. *J Clin Oncol* 2017; **35**(7 Suppl): 27.
40. Zollinger D, Sorg K, McKay-Fleisch J, *et al.* Abstract 3434: digital spatial profiling platform allows for spatially resolved, high-plex quantification of mRNA distribution and abundance on FFPE and fresh frozen tissue sections. *Cancer Res* 2018; **78**(13 Suppl): 3434.
41. Dalerba P, Kalisky T, Sahoo D, *et al.* Single-cell dissection of transcriptional heterogeneity in human colon tumors. *Nat Biotechnol* 2011; **29:** 1120–1127.
42. Rennert RC, Achrol AS, Januszyk M, *et al.* Multiple subsets of brain tumor initiating cells coexist in glioblastoma. *Stem Cells* 2016; **34:** 1702–1707.
43. Patel AP, Tirosh I, Trombetta JJ, *et al.* Single-cell RNA-seq highlights intratumoral heterogeneity in primary glioblastoma. *Science* 2014; **344:** 1396–1401.
44. Roesch A, Fukunaga-Kalabis M, Schmidt EC, *et al.* A temporarily distinct subpopulation of slow-cycling melanoma cells is required for continuous tumor growth. *Cell* 2010; **141:** 583–594.
45. Karaayvaz M, Cristea S, Gillespie SM, *et al.* Unravelling subclonal heterogeneity and aggressive disease states in TNBC through single-cell RNA-seq. *Nat Commun* 2018; **9:** 3588.
46. Becht E, de Reyniès A, Giraldo NA, *et al.* Immune and stromal classification of colorectal cancer is associated with molecular subtypes and relevant for precision immunotherapy. *Clin Cancer Res* 2016; **22:** 4057–4066.
47. Rasanen K, Sriswasdi S, Valiga A, *et al.* Comparative secretome analysis of epithelial and mesenchymal subpopulations of head and neck squamous cell carcinoma identifies S100A4 as a potential therapeutic target. *Mol Cell Proteomics* 2013; **12:** 3778–3792.
48. Kim K-T, Lee HW, Lee H-O, *et al.* Single-cell mRNA sequencing identifies subclonal heterogeneity in anti-cancer drug responses of lung adenocarcinoma cells. *Genome Biol* 2015; **16:** 127.
49. Pangeni RP, Zhang Z, Alvarez AA, *et al.* Genome-wide methylomic and transcriptomic analyses identify subtype-specific epigenetic signatures commonly dysregulated in glioma stem cells and glioblastoma. *Epigenetics* 2018; **13:** 432–448.
50. Hashimoto S, Tabuchi Y, Yurino H, *et al.* Comprehensive single-cell transcriptome analysis reveals heterogeneity in endometrioid adenocarcinoma tissues. *Sci Rep* 2017; **7:** 14225.
51. Stevens MM, Maire CL, Chou N, *et al.* Drug sensitivity of single cancer cells is predicted by changes in mass accumulation rate. *Nat Biotechnol* 2016; **34:** 1161–1167.
52. Mitra AK, Mukherjee UK, Harding T, *et al.* Single-cell analysis of targeted transcriptome predicts drug sensitivity of single cells within human myeloma tumors. *Leukemia* 2016; **30:** 1094–1102.

53. Rizvi NA, Hellmann MD, Snyder A, *et al.* Cancer immunology. Mutational landscape determines sensitivity to PD-1 blockade in non-small cell lung cancer. *Science* 2015; **348:** 124–128.
54. Gros A, Parkhurst MR, Tran E, *et al.* Prospective identification of neoantigen-specific lymphocytes in the peripheral blood of melanoma patients. *Nat Med* 2016; **22:** 433–438.
55. van Rooij N, van Buuren MM, Philips D, *et al.* Tumor exome analysis reveals neoantigen-specific T-cell reactivity in an ipilimumab-responsive melanoma. *J Clin Oncol* 2013; **31:** e439–e442.
56. Barry KC, Hsu J, Broz ML, *et al.* A natural killer-dendritic cell axis defines checkpoint therapy-responsive tumor microenvironments. *Nat Med* 2018; **24:** 1178–1191.
57. Mallett S, Fossum S, Barclay AN. Characterization of the MRC OX40 antigen of activated CD4 positive T lymphocytes – a molecule related to nerve growth factor receptor. *EMBO J* 1990; **9:** 1063–1068.
58. Calderhead DM, Buhlmann JE, van den Eertwegh AJ, *et al.* Cloning of mouse Ox40: a T cell activation marker that may mediate T-B cell interactions. *J Immunol* 1993; **151:** 5261–5271.
59. Baum PR, Gayle RB, Ramsdell F, *et al.* Molecular characterization of murine and human OX40/OX40 ligand systems: identification of a human OX40 ligand as the HTLV-1-regulated protein gp34. *EMBO J* 1994; **13:** 3992–4001.
60. Fujita T, Ukyo N, Hori T, *et al.* Functional characterization of OX40 expressed on human CD8+ T cells. *Immunol Lett* 2006; **106:** 27–33.
61. Croft M. Control of immunity by the TNFR-related molecule OX40 (CD134). *Annu Rev Immunol* 2010; **28:** 57–78.
62. Gerdes MJ, Sevinsky CJ, Sood A, *et al.* Highly multiplexed single-cell analysis of formalin-fixed, paraffin-embedded cancer tissue. *Proc Natl Acad Sci U S A* 2013; **110:** 11982–11987.
63. Schüffler PJ, Schapiro D, Giesen C, *et al.* Automatic single cell segmentation on highly multiplexed tissue images. *Cytometry A* 2015; **87:** 936–942.
64. Schapiro D, Jackson HW, Raghuraman S, *et al.* histoCAT: analysis of cell phenotypes and interactions in multiplex image cytometry data. *Nat Methods* 2017; **14:** 873–876.
65. Catena R, Özcan A, Jacobs A, *et al.* AirLab: a cloud-based platform to manage and share antibody-based single-cell research. *Genome Biol* 2016; **17:** 142.
66. Giraldo NA, Nguyen P, Engle EL, *et al.* Multidimensional, quantitative assessment of PD-1/PD-L1 expression in patients with Merkel cell carcinoma and association with response to pembrolizumab. *J Immunother Cancer* 2018; **6:** 99.
67. Amaria RN, Reddy SM, Tawbi HA, *et al.* Neoadjuvant immune checkpoint blockade in high-risk resectable melanoma. *Nat Med* 2018; **24:** 1649–1654.
68. Blank CU, Rozeman EA, Fanchi LF, *et al.* Neoadjuvant versus adjuvant ipilimumab plus nivolumab in macroscopic stage III melanoma. *Nat Med* 2018; **24:** 1655–1661.
69. Molania R, Gagnon-Bartsch JA, Dobrovic A, *et al.* A new normalization for the Nanostring nCounter gene expression assay. *bioRxiv* 2018: 374173.
70. Azizi E, Carr AJ, Plitas G, *et al.* Single-cell map of diverse immune phenotypes in the breast tumor microenvironment. *Cell* 2018; **174:** 1293–1308.e36.